

15

SYSTEM INSTABILITIES

15.1 INTRODUCTION

One of the characteristics of multiphase flows with which the engineer has to contend is that they often manifest instabilities that have no equivalent in single phase flow (see, for example, Boure *et al.* 1973, Ishii 1982, Gouesbet and Berlemont 1993). Often the result is the occurrence of large pressure, flow rate or volume fraction oscillations that, at best, disrupt the expected behavior of the multiphase flow system (and thus decrease the reliability and life of the components, Makay and Szamody 1978) and, at worst, can lead to serious flow stoppage or structural failure (see, for example, NASA 1970, Wade 1974). Moreover, in many systems (such as pump and turbine installations) the trend toward higher rotational speeds and higher power densities increases the severity of the problem because higher flow velocities increase the potential for fluid/structure interaction problems. This chapter will focus on internal flow systems and the multiphase flow instabilities that occur in them.

15.2 SYSTEM STRUCTURE

In the discussion and analysis of system stability, we shall consider that the system has been divided into its components, each identified by its index, k , as shown in figure 15.1 where each component is represented by a box. The connecting lines do not depict lengths of pipe which are themselves components. Rather the lines simply show how the components are connected. More specifically they represent specific locations at which the system has been divided up; these points are called the nodes of the system and are denoted by the index, i .

Typical and common components are pipeline sections, valves, pumps,

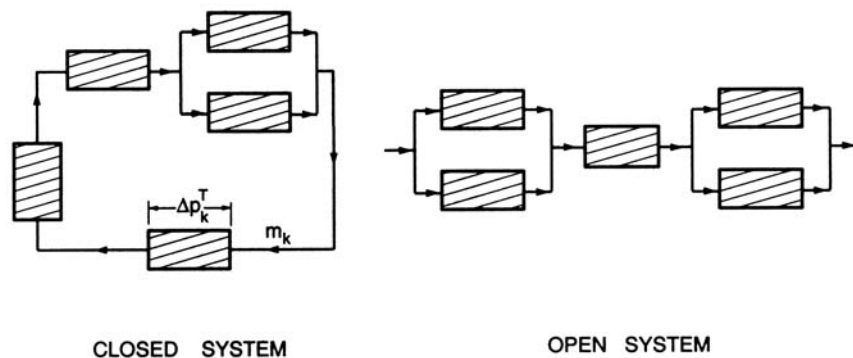


Figure 15.1. Flow systems broken into components.

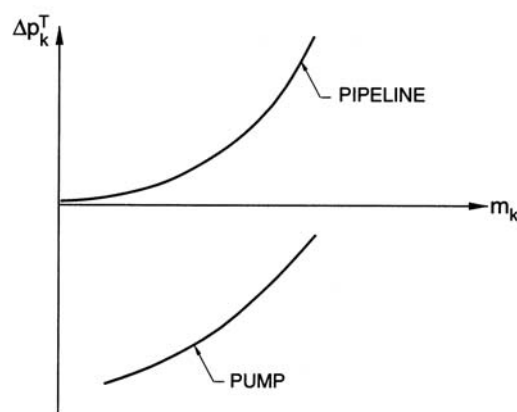


Figure 15.2. Typical component characteristics, $\Delta p_k^T(\dot{m}_k)$.

turbines, accumulators, surge tanks, boilers, and condensers. They can be connected in series and/or in parallel. Systems can be either open loop or closed loop as shown in figure 15.1. The mass flow rate through a component will be denoted by \dot{m}_k and the change in the total head of the flow across the component will be denoted by Δp_k^T defined as the total pressure at inlet minus that at discharge. (When the pressure ratios are large enough so that the compressibility of one or both of the phases must be accounted for, the analysis can readily be generalized by using total enthalpy rather than total pressure.) Then, each of the components considered in isolation will have a performance characteristic in the form of the function $\Delta p_k^T(\dot{m}_k)$ as depicted graphically in figure 15.2. We shall see that the shapes of these characteristics are important in identifying and analysing system instabilities. Some

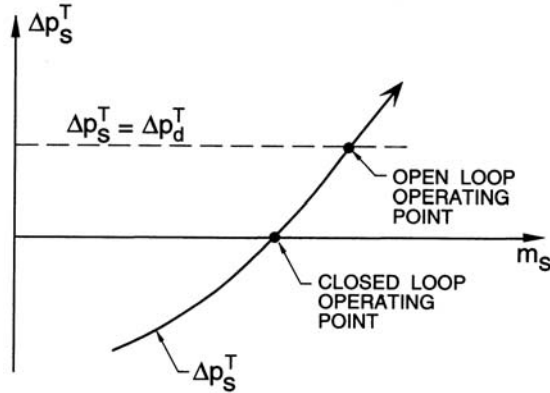


Figure 15.3. Typical system characteristic, $\Delta p_s^T(m_s)$, and operating point.

of the shapes are readily anticipated. For example, a typical single phase flow pipe section (at higher Reynolds numbers) will have a characteristic that is approximately quadratic with $\Delta p_k^T \propto \dot{m}_k^2$. Other components such as pumps, compressors or fans may have quite non-monotonic characteristics. The slope of the characteristic, R_k^* , where

$$R_k^* = \frac{1}{\rho g} \frac{d\Delta p_k^T}{d\dot{m}_k} \quad (15.1)$$

is known as the component resistance. However, unlike many electrical components, the resistance of most hydraulic components is almost never constant but varies with the flow, \dot{m}_k .

Components can readily be combined to obtain the characteristic of groups of neighboring components or the complete system. A parallel combination of two components simply requires one to add the flow rates at the same Δp^T , while a series combination simply requires that one add the Δp^T values of the two components at the same flow rate. In this way one can synthesize the total pressure drop, $\Delta p_s^T(m_s)$, for the whole system as a function of the flow rate, \dot{m}_s . Such a system characteristic is depicted in figure 15.3. For a closed system, the equilibrium operating point is then given by the intersection of the characteristic with the horizontal axis since one must have $\Delta p_s^T = 0$. An open system driven by a total pressure difference of Δp_d^T (inlet total pressure minus discharge) would have an operating point where the characteristic intersects the horizontal line at $\Delta p_s^T = \Delta p_d^T$. Since these are trivially different we can confine the discussion to the closed loop case without any loss of generality.

In many discussions, this system equilibrium is depicted in a slightly dif-

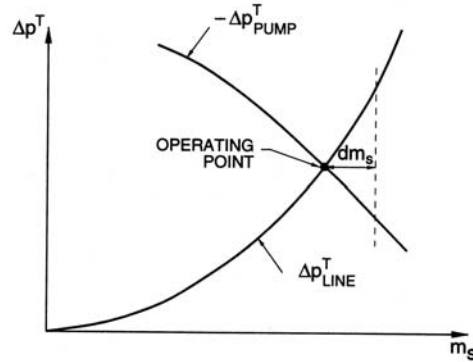


Figure 15.4. Alternate presentation of figure 15.3.

ferent but completely equivalent way by dividing the system into two series elements, one of which is the *pumping* component, $k = pump$, and the other is the *pipeline* component, $k = line$. Then the operating point is given by the intersection of the *pipeline* characteristic, Δp_{line}^T , and the *pump* characteristic, $-\Delta p_{pump}^T$, as shown graphically in figure 15.4. Note that since the total pressure increases across a pump, the values of $-\Delta p_{pump}^T$ are normally positive. In most single phase systems, this depiction has the advantage that one can usually construct a series of quadratic *pipeline* characteristics depending on the valve settings. These *pipeline* characteristics are usually simple quadratics. On the other hand the pump or compressor characteristic can be quite complex.

15.3 QUASISTATIC STABILITY

Using the definitions of the last section, a quasistatic analysis of the stability of the equilibrium operating point is usually conducted in the following way. We consider perturbing the system to a new mass flow rate dm greater than that at the operating point as shown in figure 15.4. Then, somewhat heuristically, one argues from figure 15.4 that the total pressure rise across the *pumping* component is now less than the total pressure drop across the *pipeline* and therefore the flow rate will decline back to its value at the operating point. Consequently, the particular relationship of the characteristics in figure 15.4 implies a stable operating point. If, however, the slopes of the two components are reversed (for example, Pump B of figure 15.5(a) or the operating point *C* of figure 15.5(b)) then the operating point is unstable since the increase in the flow has resulted in a *pump* total pressure that now exceeds the total pressure drop in the *pipeline*. These arguments lead to the

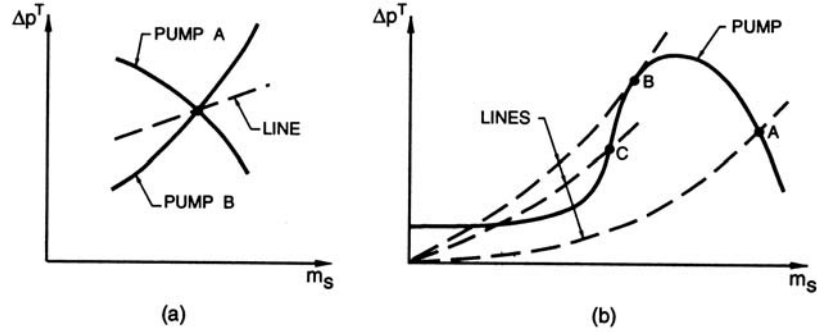


Figure 15.5. Quasistatically stable and unstable flow systems.

conclusion that the operating point is stable when the slope of the system characteristic at the operating point (figure 15.3) is positive or

$$\frac{d\Delta p_s^T}{d\dot{m}_s} > 0 \quad \text{or} \quad R_s^* > 0 \quad (15.2)$$

The same criterion can be derived in a somewhat more rigorous way by using an energy argument. Note that the net flux of flow energy out of each component is $\dot{m}_k \Delta p_k^T$. In a straight pipe this energy is converted to heat through the action of viscosity. In a pump $\dot{m}_k (-\Delta p_k^T)$ is the work done on the flow by the pump impeller. Thus the net energy flux out of the whole system is $\dot{m}_s \Delta p_s^T$ and, at the operating point, this is zero (for simplicity we discuss a closed loop system) since $\Delta p_s^T = 0$. Now, suppose, that the flow rate is perturbed by an amount $d\dot{m}_s$. Then, the new net energy flux out of the system is ΔE where

$$\Delta E = (\dot{m}_s + d\dot{m}_s) \left\{ \Delta p_s^T + d\dot{m}_s \frac{d\Delta p_s^T}{d\dot{m}_s} \right\} \approx \dot{m}_s d\dot{m}_s \frac{d\Delta p_s^T}{d\dot{m}_s} \quad (15.3)$$

Then we argue that if $d\dot{m}_s$ is positive and the perturbed system therefore dissipates more energy, then it must be stable. Under those circumstances one would have to add to the system a device that injected more energy into the system so as to sustain operation at the perturbed state. Hence the criterion 15.2 for quasistatic stability is reproduced.

15.4 QUASISTATIC INSTABILITY EXAMPLES

15.4.1 Turbomachine surge

Perhaps the most widely studied instabilities of this kind are the surge instabilities that occur in pumps, fans and compressors when the turbomachine has a characteristic of the type shown in figure 15.5(b). When the machine is operated at points such as *A* the operation is stable. However, when the turbomachine is throttled (the resistance of the rest of the system is increased), the operating point will move to smaller flow rates and, eventually, reach the point *B* at which the system is neutrally stable. Further decrease in the flow rate will result in operating conditions such as the point *C* that are quasistatically unstable. In compressors and pumps, unstable operation results in large, limit-cycle oscillations that not only lead to noise, vibration and lack of controllability but may also threaten the structural integrity of the machine. The phenomenon is known as compressor, fan or pump surge and for further details the reader is referred to Emmons *et al.*(1955), Greitzer (1976, 1981) and Brennen (1994).

15.4.2 Ledinegg instability

Two-phase flows can exhibit a range of similar instabilities. Usually, however, the instability is the result of a non-monotonic *pipeline* characteristic rather than a complex *pump* characteristic. Perhaps the best known example is the

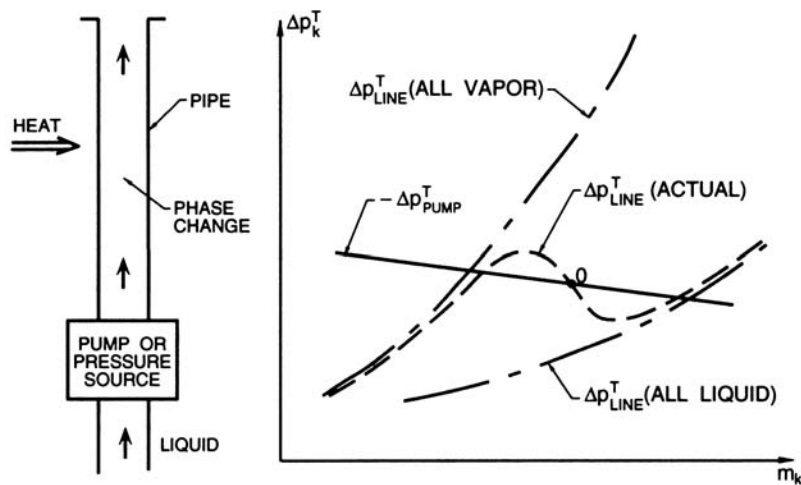


Figure 15.6. Sketch illustrating the Ledinegg instability.

Ledinegg instability (Ledinegg 1983) which is depicted in figure 15.6. This occurs in boiler tubes through which the flow is forced either by an imposed pressure difference or by a normally stable pump as sketched in figure 15.6. If the heat supplied to the boiler tube is roughly independent of the flow rate, then, at high flow rates, the flow will remain mostly liquid since, as discussed in section 8.3.2, $d\mathcal{X}/ds$ is inversely proportional to the flow rate (see equation 8.24). Therefore \mathcal{X} remains small. On the other hand, at low flow rates, the flow may become mostly vapor since $d\mathcal{X}/ds$ is large. In order to construct the $\Delta p_k^T(\dot{m}_k)$ characteristic for such a flow it is instructive to begin with the two hypothetical characteristics for all-vapor flow and for all-liquid flow. The rough form of these are shown in figure 15.6; since the frictional losses at high Reynolds numbers are proportional to $\rho u^2 = \dot{m}_k^2/\rho$, the all-vapor characteristic lies above the all-liquid line because of the different density. However, as the flow rate, \dot{m}_k , increases, the actual characteristic must make a transition from the all-vapor line to the all-liquid line, and may therefore have the non-monotonic form sketched in figure 15.6. This may lead to unstable operating points such the point O . This is the Ledinegg instability and is familiar to most as the phenomenon that occurs in a coffee percolator.

15.4.3 Geyser instability

The geyser instability that is so familiar to visitors to Yellowstone National Park and other areas of geothermal activity, has some similarities to the Ledinegg instability, but also has important differences. It has been studied in some detail in smaller scale laboratory experiments (see, for example, Nakanishi *et al.* 1978) where the parametric variations are more readily explored.

The geyser instability requires the basic components sketched in figure 15.7, namely a buried reservoir that is close to a large heat source, a vertical conduit and a near-surface supply of water that can drain into the conduit and reservoir. The geyser limit cycle proceeds as follows. During the early dormant phase of the cycle, the reservoir and conduit are filled with water that is being heated by the geothermal source. Once the water begins to boil the vapor bubbles rise up through the conduit. The hydrostatic pressure in the conduit and reservoir then drop rapidly due to the reduced mixture density in the conduit. This pressure reduction leads to explosive boiling and the eruption so widely publicized by *Old Faithful*. The eruption ends when almost all the water in the conduit and reservoir has been ejected.

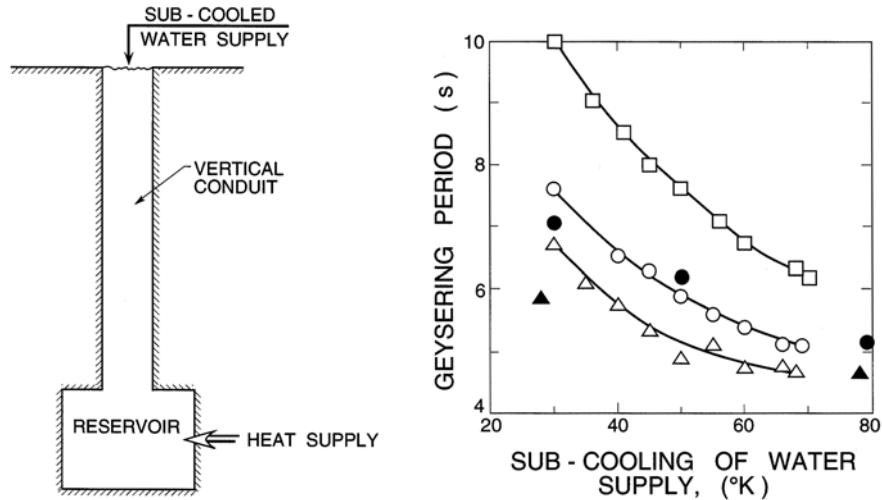


Figure 15.7. Left: The basic components for a geyser instability. Right: Laboratory measurements of geysering period as a function of heat supply (200W: □, 330W: ○, 400W: ◇) from experiments (open symbols) and numerical simulations (solid symbols). Adapted from Tae-il *et al.* (1993).

The reduced flow then allows sub-cooled water to drain into and refill the reservoir and conduit. Due to the resistance to heat transfer in the rock surrounding the reservoir, there is a significant time delay before the next load of water is heated to boiling temperatures. The long cycle times are mostly the result of low thermal conductivity of the rock (or other solid material) surrounding the reservoir and the consequent low rate of transfer of heat available to heat the sub-cooled water to its boiling temperature.

The dependence of the geysering period on the strength of the heat source and on the temperature of the sub-cooled water in the water supply is exemplified in figure 15.7 which presents results from the small scale laboratory experiments of Tae-il *et al.* (1993). That figure includes both the experimental data and the results of a numerical simulation. Note that, as expected, the geysering period decreases with increase in the strength of the heat source and with the increase in the temperature of the water supply.

15.5 CONCENTRATION WAVES

There is one phenomenon that is sometimes listed in discussions of multi-phase flow instabilities even though it is not, strictly speaking, an instability. We refer to the phenomenon of concentration wave oscillations and it is valu-

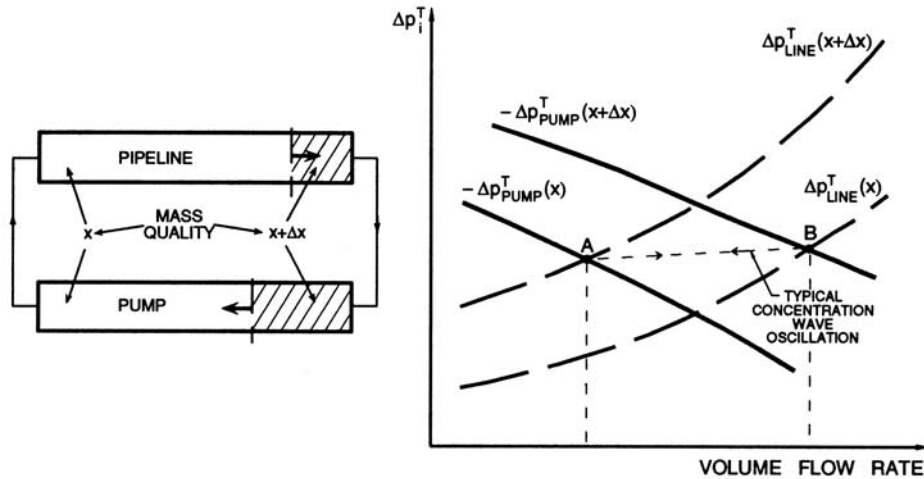


Figure 15.8. Sketch illustrating a concentration wave (density wave) oscillation.

able to include mention of the phenomenon here before proceeding to more complex matters.

Often in multiphase flow processes, one encounters a circumstance in which one part of the circuit contains a mixture with a concentration that is somewhat different from that in the rest of the system. Such an inhomogeneity may be created during start-up or during an excursion from the normal operating point. It is depicted in figure 15.8, in which the closed loop has been arbitrarily divided into a *pipeline* component and a *pump* component. As indicated, a portion of the flow has a mass quality that is larger by $\Delta\mathcal{X}$ than the mass quality in the rest of the system. Such a perturbation could be termed a concentration wave though it is also called a density wave or a continuity wave; more generally, it is known as a kinematic wave (see chapter 16). Clearly, the perturbation will move round the circuit at a speed that is close to the mean mixture velocity though small departures can occur in vertical sections in which there is significant relative motion between the phases. The mixing processes that would tend to homogenize the fluid in the circuit are often quite slow so that the perturbation may persist for an extended period.

It is also clear that the pressures and flow rates may vary depending on the location of the perturbation within the system. These fluctuations in the flow variables are termed concentration wave oscillations and they arise from the inhomogeneity of the fluid rather than from any instability in the flow. The characteristic frequency of the oscillations is simply related

to the time taken for the flow to complete one circuit of the loop (or some multiple if the number of perturbed fluid pockets is greater than unity). This frequency is usually small and its calculation often allows identification of the phenomenon.

One way in which concentration oscillations can be incorporated in the graphical presentation we have used in this chapter is to identify the component characteristics for both the mass quality, \mathcal{X} , and the perturbed quality, $\mathcal{X} + \Delta\mathcal{X}$, and to plot them using the volume flow rate rather than the mass flow rate as the abscissa. We do this because, if we neglect the compressibility of the individual phases, then the volume flow rate is constant around the circuit at any moment in time, whereas the mass flow rate differs according to the mass quality. Such a presentation is shown in figure 15.8. Then, if the perturbed body of fluid were wholly in the pipeline section, the operating point would be close to the point A . On the other hand, if the perturbed body of fluid were wholly in the pump, the operating point would be close to the point B . Thus we can see that the operating point will vary along a trajectory such as that shown by the dotted line and that this will result in oscillations in the pressure and flow rate.

In closing, we should note that concentration waves also play an important role in other more complex unsteady flow phenomena and instabilities.

15.6 DYNAMIC MULTIPHASE FLOW INSTABILITIES

15.6.1 *Dynamic instabilities*

The descriptions of the preceding sections were predicated on the frequency of the oscillations being sufficiently small for all the components to track up and down their steady state characteristics. Thus the analysis is only applicable to those instabilities whose frequencies are low enough to lie within some quasistatic range. At higher frequency, the effective resistance could become a complex function of frequency and could depart significantly from the quasistatic resistance. It follows that there may be operating points at which the total *dynamic* resistance over some range of frequencies is negative. Then the system would be dynamically unstable even though it may be quasistatically stable. Such a description of dynamic instability is instructive but overly simplistic and a more systematic approach to this issue will be detailed in section 15.7. It is nevertheless appropriate at this point to describe two examples of dynamic instabilities so that reference to these examples can be made during the description of the transfer function methodology.

15.6.2 Cavitation surge in cavitating pumps

In many installations involving a pump that cavitates, violent oscillations in the pressure and flow rate in the entire system can occur when the cavitation number is decreased to a value at which the volume of vapor bubbles within the pump becomes sufficient to cause major disruption of the flow and therefore a decrease in the total pressure rise across the pump (see section 8.4.1). While most of the detailed investigations have focused on axial pumps and inducers (Sack and Nottage 1965, Miller and Gross 1967, Kamijo *et al.* 1977, Braisted and Brennen 1980) the phenomenon has also been observed in centrifugal pumps (Yamamoto 1991). In the past this surge phenomenon was called *auto-oscillation* though the modern term *cavitation surge* is more appropriate. The phenomenon is described in detail in Brennen (1994). It can lead to very large flow rate and pressure fluctuations. For example in boiler feed systems, discharge pressure oscillations with amplitudes as high as 14 bar have been reported informally. It is a genuinely dynamic instability in the sense described in section 15.6.1, for it occurs when the slope of the pump total pressure rise/flow rate characteristic is still strongly negative and the system is therefore quasistatically stable.

As previously stated, cavitation surge occurs when the region of cavitation head loss is approached as the cavitation number is decreased. Figure 15.9

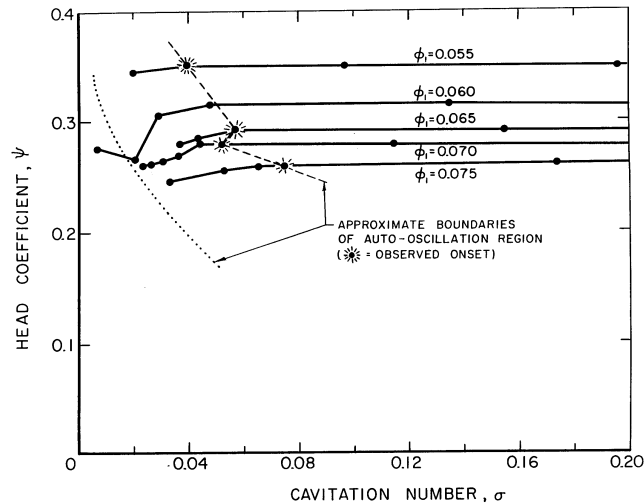


Figure 15.9. Cavitation performance of a SSME low pressure LOX pump model showing the approximate boundaries of the cavitation surge region for a pump speed of 6000 rpm (from Braisted and Brennen 1980). The flow coefficient, ϕ_1 , is based on the impeller inlet area.

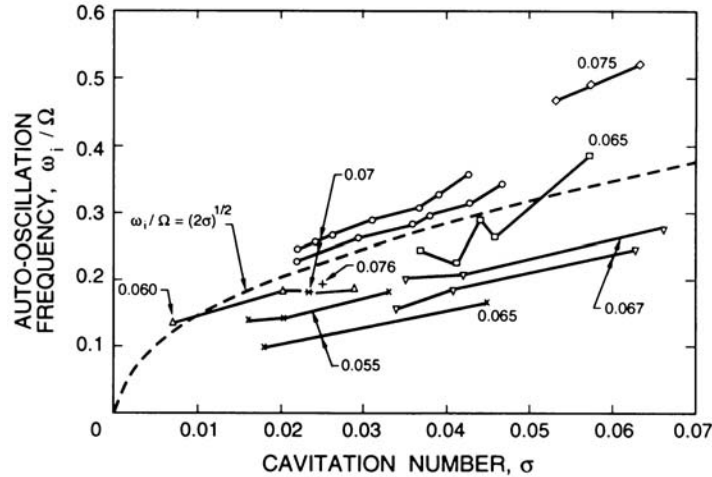


Figure 15.10. Data from Braisted and Brennen (1980) on the ratio of the frequency of cavitation surge, ω_i , to the frequency of shaft rotation, Ω , for several axial flow pumps: for SSME low pressure LOX pump models: 7.62 cm diameter: \times (9000 rpm) and $+$ (12000 rpm), 10.2 cm diameter: \odot (4000 rpm) and \square (6000 rpm); for 9° helical inducers: 7.58 cm diameter: $*$ (9000 rpm); 10.4 cm diameter: ∇ (with suction line flow straightener) and \triangle (without suction line flow straightener). The flow coefficients, ϕ_1 , are based on the impeller inlet area.

provides an example of the limits of cavitation surge taken from the work of Braisted and Brennen (1980). However, since the onset is sensitive to the detailed dynamic characteristics of the system, it would not even be wise to quote any approximate guideline for onset. Our current understanding is that the methodologies of section 15.7 are essential for any prediction of cavitation surge.

Unlike compressor surge, the frequency of cavitation surge, ω_i , scales with the shaft speed of the pump, Ω (Braisted and Brennen 1980). The ratio, ω_i/Ω , varies with the cavitation number, σ (see equation 8.31), the flow coefficient, ϕ (see equation 8.30), and the type of pump as illustrated in figure 15.10. The most systematic variation is with the cavitation number and it appears that the empirical expression

$$\omega_i/\Omega = (2\sigma)^{\frac{1}{2}} \quad (15.4)$$

provides a crude estimate of the cavitation surge frequency. Yamamoto (1991) demonstrated that the frequency also depends on the length of the suction pipe thus reinforcing the understanding of cavitation surge as a system instability.

15.6.3 Chugging and condensation oscillations

As a second example of a dynamic instability involving a two-phase flow we describe the oscillations that occur when steam is forced down a vent into a pool of water. The situation is sketched in figure 15.11. These instabilities, forms of which are known as *chugging* and *condensation oscillations*, have been most extensively studied in the context of the design of pressure suppression systems for nuclear reactors (see, for example, Wade 1974, Koch and Karwat 1976, Class and Kadlec 1976, Andeen and Marks 1978). The intent of the device is to condense steam that has escaped as a result of the rupture of a primary coolant loop and, thereby, to prevent the build-up of pressure in the containment that would have occurred as a result of uncondensed steam.

The basic components of the system are as shown in figure 15.11 and consist of a vent or pipeline of length, ℓ , the end of which is submerged to a depth, h , in the pool of water. The basic instability is illustrated in figure 15.12. At relatively low steam flow rates the rate of condensation at the steam/water interface is sufficiently high that the interface remains within the vent. However, at higher flow rates the pressure in the steam increases and the interface is forced down and out of the end of the vent. When this happens both the interface area and the turbulent mixing in the vicinity of the interface increase dramatically. This greatly increases the

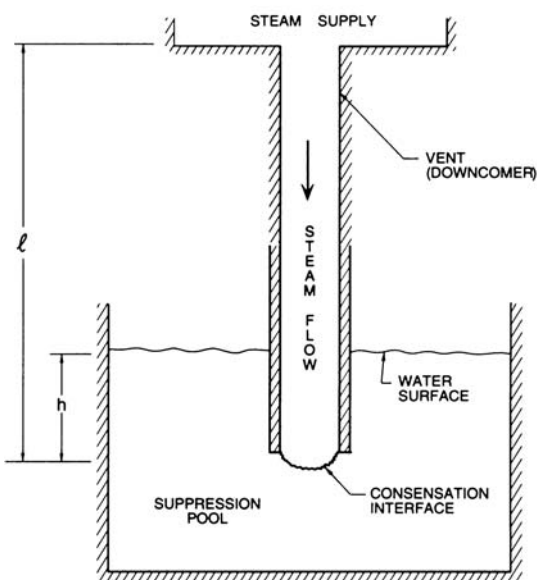


Figure 15.11. Components of a pressure suppression system.

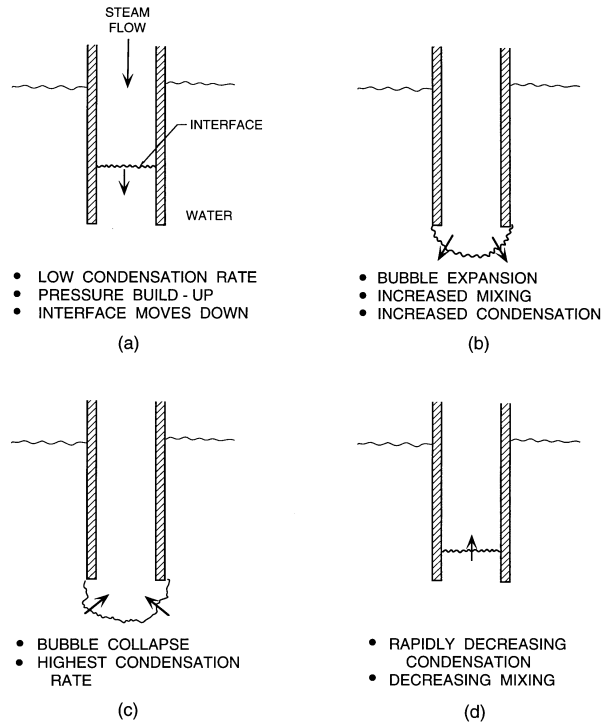


Figure 15.12. Sketches illustrating the stages of a condensation oscillation.

condensation rate which, in turn, causes a marked reduction in the steam pressure. Thus the interface collapses back into the vent, often with the same kind of violence that results from cavitation bubble collapse. Then the cycle of growth and collapse, of oscillation of the interface from a location inside the vent to one outside the end of the vent, is repeated. The phenomenon is termed condensation instability and, depending on the dominant frequency, the violent oscillations are known as *chugging* or *condensation oscillations* (Andeen and Marks 1978).

The frequency of the phenomenon tends to lock in on one of the natural modes of oscillation of the system in the absence of condensation. There are two obvious natural modes. The first, is the manometer mode of the liquid inside the end of the vent. In the absence of any steam flow, this manometer mode will have a typical small amplitude frequency, $\omega_m = (g/h)^{\frac{1}{2}}$, where g is the acceleration due to gravity. This is usually a low frequency of the order of 1Hz or less and, when the condensation instability locks into this low frequency, the phenomenon is known as *chugging*. The pressure oscillations resulting from chugging can be quite violent and can cause structural loads

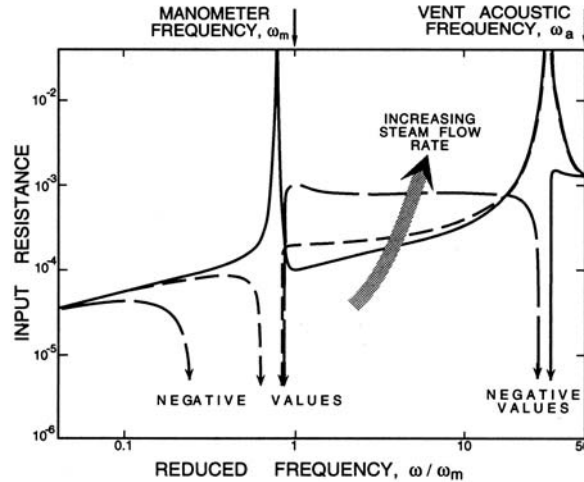


Figure 15.13. The real part of the input impedance (the input resistance) of the suppression pool as a function of the perturbation frequency for several steam flow rates. Adapted from Brennen (1979).

that are of concern to the safety engineer. Another natural mode is the first acoustic mode in the vent whose frequency, ω_a , is approximately given by $\pi c/\ell$ where c is the sound speed in the steam. There are also observations of lock-in to this higher frequency. The oscillations that result from this are known as *condensation oscillations* and tend to be of smaller amplitude than the chugging oscillations.

Figure 15.13 illustrates the results of a linear stability analysis of the suppression pool system (Brennen 1979) that was carried out using the transfer function methodology described in section 15.7. Transfer functions were constructed for the vent or downcomer, for the phase change process and for the manometer motions of the pool. Combining these, one can calculate the input impedance of the system viewed from the steam supply end of the vent. A positive input resistance implies that the system is absorbing fluctuation energy and is therefore stable; a negative input resistance implies an unstable system. In figure 15.13, the input resistance is plotted against the perturbation frequency for several steam flow rates. Note that, at low steam flow rates, the system is stable for all frequencies. However, as the steam flow rate is increased, the system first becomes unstable over a narrow range of frequencies close to the manometer frequency, ω_m . Thus chugging is predicted to occur at some critical steam flow rate. At still higher flow rates, the system also becomes unstable over a narrow range of frequencies close to the first vent acoustic frequency, ω_a ; thus the possibility of condensation

oscillations is also predicted. Note that the quasistatic input resistance at small frequencies remains positive throughout and therefore the system is quasistatically stable for all steam flow rates. Thus, chugging and condensation oscillations are true, dynamic instabilities.

It is, however, important to observe that a linear stability analysis cannot model the highly non-linear processes that occur during a *chug* and, therefore, cannot provide information on the subject of most concern to the practical engineer, namely the magnitudes of the pressure excursions and the structural loads that result from these condensation instabilities. While models have been developed in an attempt to make these predictions (see, for example, Sargis *et al.* 1979) they are usually very specific to the particular problem under investigation. Often, they must also resort to empirical information on unknown factors such as the transient mixing and condensation rates.

Finally, we note that instabilities that are similar to chugging have been observed in other contexts. For example, when steam was injected into the wake of a streamlined underwater body in order to explore underwater jet propulsion, the flow became very unstable (Kiceniuk 1952).

15.7 TRANSFER FUNCTIONS

15.7.1 *Unsteady internal flow methods*

While the details are beyond the scope of this book, it is nevertheless of value to conclude the present chapter with a brief survey of the transfer function methods referred to in section 15.6. There are two basic approaches to unsteady internal flows, namely solution in the time domain or in the frequency domain. The traditional time domain or *water-hammer* methods for hydraulic systems can and should be used in many circumstances; these are treated in depth elsewhere (for example, Streeter and Wylie 1967, 1974, Amies *et al.* 1977). They have the great advantage that they can incorporate the nonlinear convective inertial terms in the equations of fluid flow. They are best suited to evaluating the transient response of flows in long pipes in which the equations of the flow and the structure are well established. However, they encounter great difficulties when either the geometry is complex (for example inside a pump), or the fluid is complex (for example in a multiphase flow). Under these circumstances, frequency domain methods have distinct advantages, both analytically and experimentally. Specifically, unsteady flow experiments are most readily conducted by subjecting the component or device to fluctuations in the flow over a range of frequen-

cies and measuring the fluctuating quantities at inlet and discharge. The main disadvantage of the frequency domain methods is that the nonlinear convective inertial terms cannot readily be included and, consequently, these methods are only accurate for small perturbations from the mean flow. While this permits evaluation of stability limits, it does not readily allow the evaluation of the amplitude of large unstable motions. However, there does exist a core of fundamental knowledge pertaining to frequency domain methods (see for example, Pipes 1940, Paynter 1961, Brown 1967) that is summarized in Brennen (1994). A good example of the application of these methods is contained in Amies and Greene (1977).

15.7.2 Transfer functions

As in the quasistatic analyses described at the beginning of this chapter, the first step in the frequency domain approach is to identify all the flow variables that are needed to completely define the state of the flow at each of the nodes of the system. Typical flow variables are the pressure, p , (or total pressure, p^T) the velocities of the phases or components, the volume fractions, and so on. To simplify matters we count only those variables that are not related by simple algebraic expressions. Thus we do not count both the pressure and the density of a phase that behaves barotropically, nor do we count the mixture density, ρ , and the void fraction, α , in a mixture of two incompressible fluids. The minimum number of variables needed to completely define the flow at all of the nodes is called *the order of the system* and will be denoted by N . Then the state of the flow at any node, i , is denoted by the vector of state variables, $\{q_i^n\}$, $n = 1, 2 \rightarrow N$. For example, in a homogeneous flow we could choose $q_i^1 = p$, $q_i^2 = u$, $q_i^3 = \alpha$, to be the pressure, velocity and void fraction at the node i .

The next step in a frequency domain analysis is to express all the flow variables, $\{q_i^n\}$, $n = 1, 2 \rightarrow N$, as the sum of a mean component (denoted by an overbar) and a fluctuating component (denoted by a tilde) at a frequency, ω . The complex fluctuating component incorporates both the amplitude and phase of the fluctuation:

$$\{q^n(s, t)\} = \{\bar{q}^n(s)\} + Re \{ \{\tilde{q}^n(s, \omega)\} e^{i\omega t} \} \quad (15.5)$$

for $n = 1 \rightarrow N$ where i is $(-1)^{\frac{1}{2}}$ and Re denotes the real part. For example

$$p(s, t) = \bar{p}(s) + Re \{ \tilde{p}(s, \omega) e^{i\omega t} \} \quad (15.6)$$

$$\dot{m}(s, t) = \bar{\dot{m}}(s) + Re \{ \tilde{\dot{m}}(s, \omega) e^{i\omega t} \} \quad (15.7)$$

$$\alpha(s, t) = \bar{\alpha}(s) + Re \{ \tilde{\alpha}(s, \omega) e^{i\omega t} \} \quad (15.8)$$

Since the perturbations are assumed linear ($|\tilde{u}| \ll \bar{u}$, $|\tilde{m}| \ll \bar{m}$, $|\tilde{q}^n| \ll \bar{q}^n$) they can be readily superimposed, so a summation over many frequencies is implied in the above expressions. In general, the perturbation quantities, $\{\tilde{q}^n\}$, will be functions of the mean flow characteristics as well as position, s , and frequency, ω .

The utilization of transfer functions in the context of fluid systems owes much to the pioneering work of Pipes (1940). The concept is the following. If the quantities at inlet and discharge are denoted by subscripts $m = 1$ and $m = 2$, respectively, then the transfer matrix, $[T]$, is defined as

$$\{\tilde{q}_2^n\} = [T] \{\tilde{q}_1^n\} \quad (15.9)$$

It is a square matrix of order N . For example, for an order $N = 2$ system in which the independent fluctuating variables are chosen to be the total pressure, \tilde{p}^T , and the mass flow rate, \tilde{m} , then a convenient transfer matrix is

$$\begin{Bmatrix} \tilde{p}_2^T \\ \tilde{m}_2 \end{Bmatrix} = \begin{bmatrix} T_{11} & T_{12} \\ T_{21} & T_{22} \end{bmatrix} \begin{Bmatrix} \tilde{p}_1^T \\ \tilde{m}_1 \end{Bmatrix} \quad (15.10)$$

In general, the transfer matrix will be a function of the frequency, ω , of the perturbations and the mean flow conditions in the device. Given the transfer functions for each component one can then synthesize transfer functions for the entire system using a set of simple procedures described in detail in Brennen (1994). This allows one to proceed to a determination of whether or not a system is stable or unstable given the boundary conditions acting upon it.

The transfer functions for many simple components are readily identified (see Brennen 1994) and are frequently composed of impedances due to fluid friction and inertia (that primarily contribute to the real and imaginary parts of T_{12} respectively) and compliances due to fluid and structural compressibility (that primarily contribute to the imaginary part of T_{21}). More complex components or flows have more complex transfer functions that can often be determined only by experimental measurement. For example, the dynamic response of pumps can be critical to the stability of many internal flow systems (Ohashi 1968, Greitzer 1981) and consequently the transfer functions for pumps have been extensively explored (Fanelli 1972, Anderson *et al.* 1971, Brennen and Acosta 1976). Under stable operating conditions (see sections 15.3, 16.4.2) and in the absence of phase change, most pumps can be modeled with resistance, compliance and inertance elements and they

are therefore dynamically passive. However, the situation can be quite different when phase change occurs. For example, cavitating pumps are now known to have transfer functions that can cause instabilities in the hydraulic system of which they are a part. Note that under cavitating conditions, the instantaneous flow rates at inlet and discharge will be different because of the rate of change of the total volume, V , of cavitation within the pump and this leads to complex transfer functions that are described in more detail in section 16.4.2. These characteristics of cavitating pumps give rise to a variety of important instabilities such as cavitation surge (see section 15.6.2) or the Pogo instabilities of liquid-propelled rockets (Brennen 1994).

Much less is known about the transfer functions of other devices involving phase change, for example boiler tubes or vertical evaporators. As an example of the transfer function method, in the next section we consider a simple homogeneous multiphase flow.

15.7.3 Uniform homogeneous flow

As an example of a multiphase flow that exhibits the solution structure described in section 15.7.2, we shall explore the form of the solution for the inviscid, frictionless flow of a two component, gas and liquid mixture in a straight, uniform pipe. The relative motion between the two components is neglected so there is only one velocity, $u(s, t)$. Surface tension is also neglected so there is only one pressure, $p(s, t)$. Moreover, the liquid is assumed incompressible (ρ_L constant) and the gas is assumed to behave barotropically with $p \propto \rho_G^k$. Then the three equations governing the flow are the continuity equations for the liquid and for the gas and the momentum equation for the mixture which are, respectively

$$\frac{\partial}{\partial t}(1 - \alpha) + \frac{\partial}{\partial s}[(1 - \alpha)u] = 0 \quad (15.11)$$

$$\frac{\partial}{\partial t}(\rho_G \alpha) + \frac{\partial}{\partial s}(\rho_G \alpha u) = 0 \quad (15.12)$$

$$\rho \left(\frac{\partial u}{\partial t} + u \frac{\partial u}{\partial s} \right) = - \frac{\partial p}{\partial s} \quad (15.13)$$

where ρ is the usual mixture density. Note that this is a system of order $N = 3$ and the most convenient flow variables are p , u and α . These relations

yield the following equations for the perturbations:

$$-i\omega\tilde{\alpha} + \frac{\partial}{\partial s} [(1 - \bar{\alpha})\tilde{u} - \bar{u}\tilde{\alpha}] = 0 \quad (15.14)$$

$$i\omega\bar{\rho}_G\tilde{\alpha} + i\omega\bar{\alpha}\bar{\rho}_G + \bar{\rho}_G\bar{\alpha}\frac{\partial\tilde{u}}{\partial s} + \bar{\rho}_G\bar{u}\frac{\partial\tilde{\alpha}}{\partial s} + \bar{\alpha}\bar{u}\frac{\partial\tilde{\rho}_G}{\partial s} = 0 \quad (15.15)$$

$$-\frac{\partial\tilde{p}}{\partial s} = \bar{\rho} \left[i\omega\tilde{u} + \bar{u}\frac{\partial\tilde{u}}{\partial s} \right] \quad (15.16)$$

where $\tilde{\rho}_G = \tilde{p}\bar{\rho}_G/k\bar{p}$. Assuming the solution has the simple form

$$\begin{Bmatrix} \tilde{p} \\ \tilde{u} \\ \tilde{\alpha} \end{Bmatrix} = \begin{Bmatrix} P_1 e^{i\kappa_1 s} + P_2 e^{i\kappa_2 s} + P_3 e^{i\kappa_3 s} \\ U_1 e^{i\kappa_1 s} + U_2 e^{i\kappa_2 s} + U_3 e^{i\kappa_3 s} \\ A_1 e^{i\kappa_1 s} + A_2 e^{i\kappa_2 s} + A_3 e^{i\kappa_3 s} \end{Bmatrix} \quad (15.17)$$

it follows from equations 15.14, 15.15 and 15.16 that

$$\kappa_n(1 - \bar{\alpha})U_n = (\omega + \kappa_n\bar{u})A_n \quad (15.18)$$

$$(\omega + \kappa_n\bar{u})A_n + \frac{\bar{\alpha}}{k\bar{p}}(\omega + \kappa_n\bar{u})P_n + \bar{\alpha}\kappa_n U_n = 0 \quad (15.19)$$

$$\bar{\rho}(\omega + \kappa_n\bar{u})U_n + \kappa_n P_n = 0 \quad (15.20)$$

Eliminating A_n , U_n and P_n leads to the dispersion relation

$$(\omega + \kappa_n\bar{u}) \left[1 - \frac{\bar{\alpha}\bar{\rho}}{k\bar{p}} \frac{(\omega + \kappa_n\bar{u})^2}{\kappa_n^2} \right] = 0 \quad (15.21)$$

The solutions to this dispersion relation yield the following wavenumbers and velocities, $c_n = -\omega/\kappa_n$, for the perturbations:

- $\kappa_1 = -\omega/\bar{u}$ which has a wave velocity, $c_0 = \bar{u}$. This is a purely kinematic wave, a concentration wave that from equations 15.18 and 15.20 has $U_1 = 0$ and $P_1 = 0$ so that there are no pressure or velocity fluctuations associated with this type of wave. In other, more complex flows, kinematic waves may have some small pressure and velocity perturbations associated with them and their velocity may not exactly correspond with the mixture velocity but they are still called kinematic waves if the major feature is the concentration perturbation.
- $\kappa_2, \kappa_3 = -\omega/(\bar{u} \pm c)$ where c is the sonic speed in the mixture, namely $c = (k\bar{p}/\bar{\alpha}\bar{\rho})^{1/2}$. Consequently, these two modes have wave speeds $c_2, c_3 = \bar{u} \pm c$ and are the two acoustic waves traveling downstream and upstream respectively.

Finally, we list the solution in terms of three unknown, complex constants P_2 , P_3 and A_1 :

$$\begin{pmatrix} \tilde{p} \\ \tilde{u} \\ \tilde{\alpha} \end{pmatrix} = \begin{bmatrix} 0 & e^{i\kappa_2 s} & e^{i\kappa_3 s} \\ 0 & -e^{i\kappa_2 s}/\bar{\rho}c & e^{i\kappa_3 s}/\bar{\rho}c \\ e^{i\kappa_1 s} & -(1-\bar{\alpha})e^{i\kappa_2 s}/\bar{\rho}c^2 & -(1-\bar{\alpha})e^{i\kappa_3 s}/\bar{\rho}c^2 \end{bmatrix} \begin{pmatrix} A_1 \\ P_2 \\ P_3 \end{pmatrix} \quad (15.22)$$

and the transfer function between two locations $s = s_1$ and $s = s_2$ follows by eliminating the vector $\{A_1, P_2, P_3\}$ from the expressions 15.22 for the state vectors at those two locations.

Transfer function methods for multiphase flow are nowhere near as well developed as they are for single phase flows but, given the number and ubiquity of instability problems in multiphase flows (Ishii 1982), it is inevitable that these methods will gradually develop into a tool that is useful in a wide spectrum of applications.